Double Horizon Peridynamics

Zhenghao Yang[1], Erkan Oterkus[2,*], Selda Oterkus[2], Chien-Ching Ma[1]

[1]Department of Mechanical Engineering, National Taiwan University, Taipei, Taiwan

[2]PeriDynamics Research Centre, Department of Naval Architecture, Ocean and Marine Engineering, University of Strathclyde, Glasgow, United Kingdom

*Corresponding author: erkan.oterkus@strath.ac.uk

Abstract

In this study, a new double horizon peridynamics formulation was introduced by utilising two horizons instead of one as in traditional peridynamics. The new approach allows utilisation of large horizon sizes by controlling the size of the inner horizon size. To demonstrate the capability of the current approach, four different numerical cases were examined by considering static and dynamic conditions, different boundary and initial conditions, and different outer and inner horizon size values. For both static and dynamic cases, it was observed that as the inner horizon decreases, peridynamic solutions converge to classical continuum mechanics solutions even by using a larger horizon size value. Therefore, the proposed approach can serve as an alternative approach to improve computational efficiency of peridynamic simulations by obtaining accurate results with larger horizon sizes.

Keywords: Peridynamics; non-local; horizon; continuum mechanics

1 Introduction

Although classical continuum mechanics has been widely used for the analysis of materials and structures under external loading conditions, equations of classical continuum mechanics are not suitable to represent situations including discontinuities such as cracks since spatial derivatives in classical continuum mechanics equations are not defined along the crack boundaries. Silling [1] introduced peridynamics with the intention to overcome limitations of classical continuum mechanics formulation. By using integro-differential equations without spatial derivatives, peridynamics has become a powerful approach for predicting of crack evolution in materials and structures [2]. Rather than using mesh-based or semi-analytical approaches [3], peridynamics formulation is usually numerically implemented by utilising meshless approach. There has been significant progress on peridynamics especially during recent years. Amongst numerous studies in the field, Vazic et. al. [4] demonstrated the superior capability of peridynamics in fracture analysis by investigating the interacting of macro and micro cracks. De Meo et. al. [5] predicted pit-to-crack transition process within peridynamic framework. Imachi et. al. [6] performed dynamic crack arrest analysis by using peridynamics. Ozdemir et. al. [7] used peridynamics to investigate functionally graded materials and their dynamic fracture behaviour. Liu et. al. [8] analysed fracture of zigzag graphene sheets by creating an ordinary state-based peridynamic model. Huang et. al. [9] extended the capability of peridynamics for visco-hyperelastic materials. Diehl et. al. [10] presented a review of benchmark experiments for peridynamic models. Zhou and Yao [11] proposed a new concept of smoothed bond-based peridynamics. Prakash and Stewart [12] demonstrated how to use a multi-threaded method to assemble a sparse stiffness matrix for quasi-static problems of peridynamics. Naumenko et. al. [13] compared experimental and peridynamic results for damage patterns in float glass plates. Yan et. al. [14] used peridynamics to model soil desiccation. Hidayat et. al. [15] provided a review about relationship between meshfree methods and peridynamics. Guski et. al. [16] utilised peridynamics to investigate plasma sprayed coatings for SOFC sealing applications. Kefal et. al. [17] demonstrated how to use peridynamics for topology optimisation of cracked structures. There have been also many studies presenting peridynamic formulations for beams and plates to model isotropic materials [18-22], functionally graded materials [23-28] and composite materials [29,30]. Peridynamics has also been extended to model other physical fields. Mikata [31] presented peridynamic formulations for fluid mechanics and acoustics. Diyaroglu et. al. [32] introduced peridynamic wetness approach to be utilised for the analysis of moisture concentration in electronic packages.

This is a peer reviewed, accepted author manuscript of the following research article: Yang, Z., Oterkus, E., Oterkus, S., & Ma, C-C. (Accepted/In press - 18 April 2023). Double horizon peridynamics. *Mathematics and Mechanics of Solids*.

Martowicz et. al. [33] created a thermomechanical model to investigate phase transformation in shape memory alloys.

An important aspect of peridynamics is its length scale parameter, horizon, which doesn't exist in classical continuum mechanics formulation. Dorduncu and Madenci [34] presented finite element implementation of ordinary state-based peridynamics having variable horizon. Madenci et. al. [35] developed weak form of bond-associated non-ordinary state-based peridynamics formulation for uniform or non-uniform discretization without experiencing zero-energy mode problem. A comprehensive investigation on how to choose horizon size in bond-based peridynamics and state-based peridynamics is given in Bobaru and Hu [36] and Wang et. al. [37], respectively. In this study, a new peridynamic formulation, double horizon peridynamics, is proposed which utilises two horizons for each material point instead of one horizon as in traditional peridynamics formulation. Since simulations based traditional peridynamics can take significant computational time for some cases if a large horizon size and/or refined discretization are utilized, this new formulation can allow improvement of numerical accuracy in peridynamic simulations with less computational time. This formulation is different than "dual horizon peridynamics" formulation which uses two different horizons for two interacting material points [38-41]. The details of the "double horizon peridynamics" formulation is given in Section 2. How to treat boundary conditions is explained in Section 3. Analytical solutions for various different boundary conditions under static or dynamic conditions are given in Sections 4 and 5. Some numerical results are presented in Section 6 and conclusions of the study are given Section 7.

2 Double horizon peridynamic formulation

2.1 Traditional Peridynamics

The equation of motion (EoM) for a 1-Dimensional (1D) rod in Classical Continuum Mechanics (CCM) can be written as

$$\rho \frac{\partial^2 u}{\partial t^2}(x,t) = E \frac{\partial^2 u}{\partial x^2} + b(x,t) \tag{1}$$

PD EoM for 1D bar can be obtained by converting the local term in Eq. (1) into nonlocal form by utilizing Taylor expansion. Performing Taylor expansion with respect to displacement function u about a particular material point x and absorbing higher order terms within $O(*)$ function yields

$$u(x+\xi) - u(x) = \frac{\partial u}{\partial x}\xi + \frac{1}{2}\frac{\partial^2 u}{\partial x^2}\xi^2 + \frac{1}{3!}\frac{\partial^3 u}{\partial x^3}\xi^3 + O(\xi^4) \tag{2}$$

Considering x as fixed, multiplying each term of Eq. (2) by the influence function $1/|\xi|$ and integrating over the PD horizon results in

$$\int_{-\delta}^{\delta} \frac{u(x+\xi)-u(x)}{|\xi|} d\xi = \frac{\partial u}{\partial x}\int_{-\delta}^{\delta} \operatorname{sgn}(\xi) d\xi + \frac{1}{2}\frac{\partial^2 u}{\partial x^2}\int_{-\delta}^{\delta} |\xi| d\xi + \frac{1}{3!}\frac{\partial^3 u}{\partial x^3}\int_{-\delta}^{\delta} \xi^2 \operatorname{sgn}(\xi) d\xi + \int_{-\delta}^{\delta} O(|\xi^3|) d\xi \tag{3}$$

which gives

$$\frac{\partial^2 u}{\partial x^2} = \frac{2}{\delta^2}\int_{-\delta}^{\delta} \frac{u(x+\xi)-u(x)}{|\xi|} d\xi + O(\delta^4) \tag{4}$$

Substituting Eq. (4) into Eq. (1) yields

$$\rho \frac{\partial^2 u}{\partial t^2}(x,t) = \frac{2E}{\delta^2}\int_{-\delta}^{\delta} \frac{u(x+\xi)-u(x)}{|\xi|} d\xi + b(x,t) + O(\delta^4) \tag{5}$$

It reduces to the classic PD EoM if we eliminate the residual term in the above equation such that

$$\rho\frac{\partial^2 u}{\partial t^2}(x,t)=\frac{2EA}{\delta^2}\int_{-\delta}^{\delta}\frac{u(x+\xi)-u(x)}{|\xi|}d\xi+b(x,t) \tag{6}$$

2.2 Double Horizon Peridynamics

One can observe that the classical PD EoM, Eq. (6) identically converges to that of CCM, Eq. (1) if and only if when the horizon size, δ, tends to zero. However, horizon as an important parameter which gives PD a nonlocal character and should take up a value of finite length in general. A numerical approach is usually utilised to solve PD EoM. In order to consistently match PD with CCM, a very small horizon size can be chosen, but this brings the price of losing nonlocality and significant computational time. On the other hand, choosing large horizon may avoid these issues but causes less accurate results. In order to overcome this contradiction, double horizon peridynamics formulation can be introduced in the PD EoM.

Consider a small inner horizon inside the original horizon as shown in Figure 1.

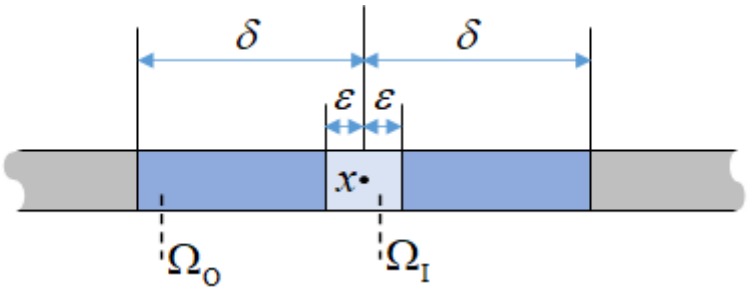

Figure 1. The inner horizon Ω_I and the outer horizon Ω_O in the double horizon peridynamic formulation.

First, let us consider the integration over the inner horizon Ω_I. By making analogy with the derivation of equations from Eq. (2) to (4) by replacing δ with ε, one can obtain

$$\frac{\partial^2 u}{\partial x^2}=\frac{2}{\varepsilon^2}\int_{-\varepsilon}^{\varepsilon}\frac{u(x+\xi)-u(x)}{|\xi|}d\xi+O(\varepsilon^4) \tag{7}$$

Note that the inner horizon size ε can be chosen arbitrarily small, such that $O(\varepsilon^4)\ll O(\delta^4)$

Next, let us consider the integration over the outer horizon Ω_O. Multiplying each term in Eq. (2) by the influence function $1/|\xi|$ gives

$$\frac{u(x+\xi)-u(x)}{|\xi|}=\frac{\partial u}{\partial x}\mathrm{sgn}(\xi)+\frac{1}{2}\frac{\partial^2 u}{\partial x^2}|\xi|+\frac{1}{3!}\frac{\partial^3 u}{\partial x^3}\xi^2\,\mathrm{sgn}(\xi)+O(|\xi^3|) \tag{8}$$

Note that when ξ varies over the outer horizon, the residual term ranges as

$$|O(|\varepsilon^3|)|\le|O(|\xi^3|)|\le|O(|\delta^3|)| \quad \forall\xi\in\Omega_O \tag{9}$$

In order to reduce the residual to be consistent with that of the inner horizon, multiplying Eq. (8) by $\left|\frac{\varepsilon^3}{\xi^3}\right|$ implies

$$\left|\frac{\varepsilon^3}{\xi^3}\right|\frac{u(x+\xi)-u(x)}{|\xi|}=\frac{\partial u}{\partial x}\left|\frac{\varepsilon^3}{\xi^3}\right|\mathrm{sgn}(\xi)+\frac{1}{2}\frac{\partial^2 u}{\partial x^2}\left|\frac{\varepsilon^3}{\xi^3}\right||\xi|+\frac{1}{3!}\frac{\partial^3 u}{\partial x^3}\xi^2\left|\frac{\varepsilon^3}{\xi^3}\right|\mathrm{sgn}(\xi)+O(|\varepsilon^3|) \tag{10}$$

Now considering x as fixed and integrating over the outer horizon results in

$$\int_{\Omega_O}\left|\frac{\varepsilon^3}{\xi^3}\right|\frac{u(x+\xi)-u(x)}{|\xi|}d\xi=\frac{\partial u}{\partial x}\int_{\Omega_O}\left|\frac{\varepsilon^3}{\xi^3}\right|\mathrm{sgn}(\xi)d\xi+\frac{1}{2}\frac{\partial^2 u}{\partial x^2}\int_{\Omega_O}\left|\frac{\varepsilon^3}{\xi^3}\right||\xi|d\xi \\ +\frac{1}{3!}\frac{\partial^3 u}{\partial x^3}\int_{\Omega_O}\xi^2\left|\frac{\varepsilon^3}{\xi^3}\right|\mathrm{sgn}(\xi)d\xi+\int_{\Omega_O}O\left(\left|\varepsilon^3\right|\right)d\xi \tag{11}$$

Ignoring residual gives

$$\frac{\partial^2 u}{\partial x^2}=\frac{\delta}{\varepsilon^2(\delta-\varepsilon)}\left[\int_{-\delta}^{-\varepsilon}\left|\frac{\varepsilon^3}{\xi^3}\right|\frac{u(x+\xi)-u(x)}{|\xi|}d\xi+\int_{\varepsilon}^{\delta}\left|\frac{\varepsilon^3}{\xi^3}\right|\frac{u(x+\xi)-u(x)}{|\xi|}d\xi\right] \tag{12}$$

Introducing two weight functions ω_I and ω_O for inner and outer horizon, respectively, such that

$$\omega_I+\omega_O=1 \tag{13}$$

and combining Eq. (7) with (12) gives

$$\frac{\partial^2 u}{\partial x^2}=\omega_I\frac{2}{\varepsilon^2}\int_{-\varepsilon}^{\varepsilon}\frac{u(x+\xi)-u(x)}{|\xi|}d\xi+\omega_O\frac{\delta}{\varepsilon^2(\delta-\varepsilon)}\left[\int_{-\delta}^{-\varepsilon}\left|\frac{\varepsilon^3}{\xi^3}\right|\frac{u(x+\xi)-u(x)}{|\xi|}d\xi+\int_{\varepsilon}^{\delta}\left|\frac{\varepsilon^3}{\xi^3}\right|\frac{u(x+\xi)-u(x)}{|\xi|}d\xi\right] \tag{14}$$

in which the weight functions can be chosen by considering each horizon size in proportion to the total horizon size as

$$\omega_I=\frac{\varepsilon}{\delta}\quad\omega_O=\frac{\delta-\varepsilon}{\delta} \tag{15}$$

Coupling Eq. (15) with (14) and substituting into (1) yields the refined PD EoM for 1D bar as

$$\rho\frac{\partial^2 u}{\partial t^2}(x,t)=\frac{2E}{\delta\varepsilon}\int_{-\varepsilon}^{\varepsilon}\frac{u(x+\xi)-u(x)}{|\xi|}d\xi+\frac{E}{\varepsilon^2}\left[\int_{-\delta}^{-\varepsilon}\left|\frac{\varepsilon^3}{\xi^3}\right|\frac{u(x+\xi)-u(x)}{|\xi|}d\xi+\int_{\varepsilon}^{\delta}\left|\frac{\varepsilon^3}{\xi^3}\right|\frac{u(x+\xi)-u(x)}{|\xi|}d\xi\right]+b(x,t) \tag{16}$$

Note that when the inner horizon size equals to the outer horizon size, $\varepsilon=\delta$, Eq. (16) reduces to the traditional PD form.

3. Boundary Conditions

From PD point of view, except damage situation, each material point must be completely embedded in its PD influence domain. Moreover, for those material points adjacent to the boundary, whose domain is incomplete, it is necessary to introduce fictitious region outside the boundary such that the completeness of PD Equation of Motion (EoM) is ensured. The width of fictitious region can be chosen as equal to the horizon size δ, as shown in Fig. 2. Two types of BCs and their implementation in PD framework are explained below.

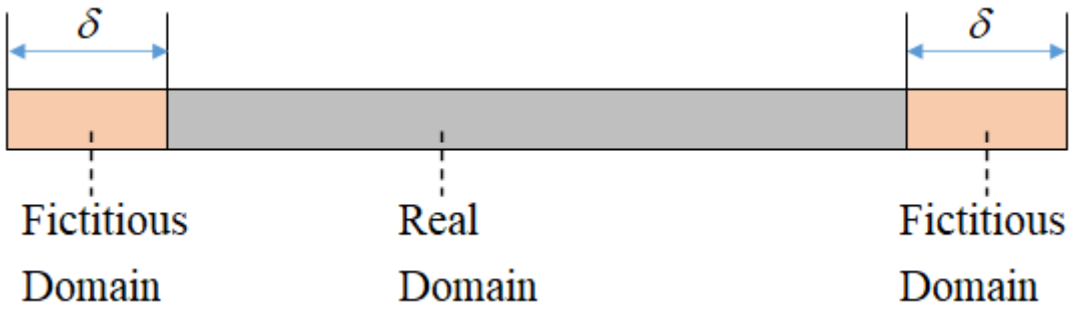

Figure 2. Real and fictitious domains

3.1 Fixed Boundary Conditions

Recall the EoM in classical elasticity:

$$\rho\frac{\partial^2 u}{\partial t^2}(x,t)=E\frac{\partial^2 u(x,t)}{\partial x^2}+b(x,t)\quad 0\le x\le L \tag{17}$$

Suppose the body is constrained at $x=0$ such that $u(0,t)\equiv 0$, the representation of Eq. (1) at this point is:

$$E\frac{\partial^2 u(x,t)}{\partial x^2}\bigg|_{x=0}=0 \tag{18}$$

One can obtain by performing central difference for Eq. (18) that

$$E\frac{u(-\Delta x,t)-2u(0,t)+u(\Delta x,t)}{(\Delta x)^2}=0 \tag{19}$$

where Δx is incremental distance. Simplifying Eq. (19) and swapping the difference notation Δx by ξ leads to

$$u(-\xi,t)=-u(\xi,t)\quad 0<\xi<\delta \tag{20}$$

Here, the material point $x=-\xi$ lies in the fictitious region and Eq. (20) ensures that the fixed BC is satisfied for PD EoM.

3.2 Neumann Boundary Conditions

Suppose the body is subjected to a concentrated load of $p(t)$ at $x=L$. In classical elasticity theory, the boundary condition can be represented as

$$\sigma(L,t)=E\frac{\partial u(x,t)}{\partial x}\bigg|_{x=L}=p(t) \tag{21}$$

Again, performing central difference with respect to u gives

$$E\frac{u(L+\Delta x,t)-u(L-\Delta x,t)}{2\Delta x}=p(t) \tag{22}$$

After performing some algebra and rearranging the central difference notation according to PD convention, one can obtain that

$$u\left(L+\xi,t\right)=2\frac{p\left(t\right)}{E}\xi+u\left(L-\xi,t\right)\quad 0<\xi<\delta \tag{23}$$

Note that, $p(t)$ can be eliminated from Eq. (23) and absorbed in Eq. (16) if it is considered as the body force operated by Dirac delta. According to this point of view, Eq. (23) reduces to

$$u\left(L+\xi,t\right)=u\left(L-\xi,t\right)\quad 0<\xi<\delta \tag{24}$$

and Eq. (24) is called the free boundary condition relationship in PD framework.

4. Analytic Solutions for Static Problems

4.1 Fixed-Fixed Rod

Consider a rod subjected to fixed-fixed boundary condition and arbitrary distributed loading as shown in Fig. 3.

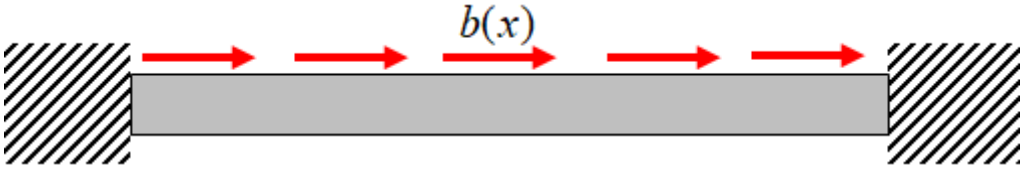

Figure 3. Rod subjected to fixed-fixed boundary condition and arbitrary distributed loading

The length of the bar is denoted as L and Young's modulus is E. As explained earlier, the PD EoM and BCs can be expressed as

$$\frac{2E}{\delta\varepsilon}\int_{-\varepsilon}^{\varepsilon}\frac{u\left(x+\xi\right)-u\left(x\right)}{\left|\xi\right|}d\xi+\frac{E}{\varepsilon^2}\left[\int_{-\delta}^{-\varepsilon}\left|\frac{\varepsilon^3}{\xi^3}\right|\frac{u\left(x+\xi\right)-u\left(x\right)}{\left|\xi\right|}d\xi+\int_{\varepsilon}^{\delta}\left|\frac{\varepsilon^3}{\xi^3}\right|\frac{u\left(x+\xi\right)-u\left(x\right)}{\left|\xi\right|}d\xi\right]+b\left(x\right)=0 \tag{25}$$

$$\begin{cases}u\left(-\xi\right)=-u\left(\xi\right)\\ u\left(L+\xi\right)=-u\left(L-\xi\right)\end{cases}\quad 0\le\xi\le\delta \tag{26a, b}$$

According to the completeness characteristic of a trigonometric system, it is reasonable to assume that the displacement function accommodates in the vector space spanned by trigonometric functions, i.e.

$$u\left(x\right)\in Span\left\{\begin{matrix}\frac{1}{\sqrt{2}}, & \cos\left(s_1x\right), & \cos\left(s_2x\right), & \cos\left(s_3x\right), & ...\\ & \sin\left(s_1x\right), & \sin\left(s_2x\right), & \sin\left(s_3x\right), & ...\end{matrix}\right\} \tag{27}$$

which can be expressed as a linear combination in terms of the bases as follows:

$$u\left(x\right)=\frac{a_0}{2}+\sum_{n=1}^{\infty}a_n\cos\left(s_nx\right)+b_n\sin\left(s_nx\right) \tag{28}$$

Substituting Eq. (28) into (26a) yields

$$\frac{a_0}{2}+\sum_{n=1}^{\infty}a_n\cos\left(-s_n\xi\right)+b_n\sin\left(-s_n\xi\right)=-\left[\frac{a_0}{2}+\sum_{n=1}^{\infty}a_n\cos\left(s_n\xi\right)+b_n\sin\left(s_n\xi\right)\right] \tag{29}$$

Without considering rigid body motion, one can obtain that

$$u(x)=\sum_{n=1}^{\infty}b_n\sin(s_n x) \tag{30}$$

Substituting Eq. (30) into (26b) yields

$$\sum_{n=1}^{\infty}b_n\sin\left[s_n(L+\xi)\right]=-\sum_{n=1}^{\infty}b_n\sin\left[s_n(L-\xi)\right] \tag{31}$$

which gives

$$\sum_{n=1}^{\infty}b_n\sin(s_nL)\cos(s_n\xi)=0 \quad \Rightarrow \quad s_n=\frac{n\pi}{L} \tag{32}$$

Plugging Eq. (32) back into (30) implies

$$u(x)=\sum_{n=1}^{\infty}b_n\sin\left(\frac{n\pi}{L}x\right) \tag{33}$$

One can obtain that

$$\begin{aligned}\int_{-\varepsilon}^{\varepsilon}\frac{u(x+\xi)-u(x)}{|\xi|}d\xi&=\sum_{n=1}^{\infty}b_n\int_{-\varepsilon}^{\varepsilon}\frac{1}{|\xi|}\left[\sin\left(\frac{n\pi(x+\xi)}{L}\right)-\sin\left(\frac{n\pi x}{L}\right)\right]d\xi\\&=\sum_{n=1}^{\infty}b_n\sin\left(\frac{n\pi x}{L}\right)\int_{-\varepsilon}^{\varepsilon}\frac{1}{|\xi|}\left[\cos\left(\frac{n\pi\xi}{L}\right)-1\right]d\xi\end{aligned} \tag{34}$$

Similarly,

$$\begin{aligned}&\int_{-\delta}^{-\varepsilon}\left|\frac{\varepsilon^3}{\xi^3}\right|\frac{u(x+\xi)-u(x)}{|\xi|}d\xi+\int_{\varepsilon}^{\delta}\left|\frac{\varepsilon^3}{\xi^3}\right|\frac{u(x+\xi)-u(x)}{|\xi|}d\xi\\&=\int_{-\delta}^{\delta}\left|\frac{\varepsilon^3}{\xi^3}\right|\frac{u(x+\xi)-u(x)}{|\xi|}d\xi-\int_{-\varepsilon}^{\varepsilon}\left|\frac{\varepsilon^3}{\xi^3}\right|\frac{u(x+\xi)-u(x)}{|\xi|}d\xi\\&=\sum_{n=1}^{\infty}b_n\int_{-\delta}^{\delta}\left|\frac{\varepsilon^3}{\xi^4}\right|\left[\sin\left(\frac{n\pi}{L}(x+\xi)\right)-\sin\left(\frac{n\pi}{L}x\right)\right]d\xi-\sum_{n=1}^{\infty}b_n\int_{-\varepsilon}^{\varepsilon}\left|\frac{\varepsilon^3}{\xi^4}\right|\left[\sin\left(\frac{n\pi}{L}(x+\xi)\right)-\sin\left(\frac{n\pi}{L}x\right)\right]d\xi\\&=\sum_{n=1}^{\infty}b_n\sin\left(\frac{n\pi x}{L}\right)\int_{-\delta}^{\delta}\left|\frac{\varepsilon^3}{\xi^4}\right|\left[\cos\left(\frac{n\pi\xi}{L}\right)-1\right]d\xi-\sum_{n=1}^{\infty}b_n\sin\left(\frac{n\pi x}{L}\right)\int_{-\varepsilon}^{\varepsilon}\left|\frac{\varepsilon^3}{\xi^4}\right|\left[\cos\left(\frac{n\pi\xi}{L}\right)-1\right]d\xi\\&=\sum_{n=1}^{\infty}b_n\sin\left(\frac{n\pi x}{L}\right)\left\{\int_{-\delta}^{-\varepsilon}\left|\frac{\varepsilon^3}{\xi^4}\right|\left(\cos\frac{n\pi\xi}{L}-1\right)d\xi+\int_{\varepsilon}^{\delta}\left|\frac{\varepsilon^3}{\xi^4}\right|\left(\cos\frac{n\pi\xi}{L}-1\right)d\xi\right\}\end{aligned} \tag{35}$$

Substituting Eq. (34) and (35) into (25) yields

$$\sum_{n=1}^{\infty}b_n\sin\left(\frac{n\pi x}{L}\right)\left\{\frac{2E}{\delta\varepsilon}\int_{-\varepsilon}^{\varepsilon}\frac{1}{|\xi|}\left[\cos\left(\frac{n\pi\xi}{L}\right)-1\right]d\xi+\frac{E}{\varepsilon^2}\left[\int_{-\delta}^{-\varepsilon}\left|\frac{\varepsilon^3}{\xi^4}\right|\left(\cos\frac{n\pi\xi}{L}-1\right)d\xi+\int_{\varepsilon}^{\delta}\left|\frac{\varepsilon^3}{\xi^4}\right|\left(\cos\frac{n\pi\xi}{L}-1\right)d\xi\right]\right\}=-b(x) \tag{36}$$

According to the orthogonal property of trigonometric functions, the coefficients can be determined as

$$b_n = -\frac{2}{L}\frac{\int_0^L b(x)\sin\frac{n\pi x}{L}dx}{\frac{2E}{\delta\varepsilon}\int_{-\varepsilon}^{\varepsilon}\frac{1}{|\xi|}\left(\cos\frac{n\pi\xi}{L}-1\right)d\xi+\frac{E}{\varepsilon^2}\left[\int_{-\delta}^{-\varepsilon}\left|\frac{\varepsilon^3}{\xi^4}\right|\left(\cos\frac{n\pi\xi}{L}-1\right)d\xi+\int_{\varepsilon}^{\delta}\left|\frac{\varepsilon^3}{\xi^4}\right|\left(\cos\frac{n\pi\xi}{L}-1\right)d\xi\right]} \tag{37}$$

Hence, the analytical PD solution is

$$u(x)=\sum_{n=1}^{\infty}\frac{2}{L}\frac{\int_0^L b(x)\sin\frac{n\pi x}{L}dx\sin\left(\frac{n\pi x}{L}\right)}{\frac{2E}{\delta\varepsilon}\int_{-\varepsilon}^{\varepsilon}\frac{1}{|\xi|}\left(1-\cos\frac{n\pi\xi}{L}\right)d\xi+\frac{E}{\varepsilon^2}\left[\int_{-\delta}^{-\varepsilon}\left|\frac{\varepsilon^3}{\xi^4}\right|\left(1-\cos\frac{n\pi\xi}{L}\right)d\xi+\int_{\varepsilon}^{\delta}\left|\frac{\varepsilon^3}{\xi^4}\right|\left(1-\cos\frac{n\pi\xi}{L}\right)d\xi\right]} \tag{38}$$

Note that when $\varepsilon=\delta$, Eq. (38) reduces to analytical solution for classical PD theory as

$$u(x)=\sum_{n=1}^{\infty}\frac{\delta^2}{EL}\frac{\int_0^L b(x)\sin\frac{n\pi x}{L}dx}{\int_{-\delta}^{\delta}\frac{1}{|\xi|}\left(1-\cos\frac{n\pi\xi}{L}\right)d\xi}\sin\left(\frac{n\pi x}{L}\right) \tag{39}$$

4.2 Fixed-Free Rod

Consider a rod subjected to fixed-free boundary condition and arbitrary distributed loading as shown in Fig. 4.

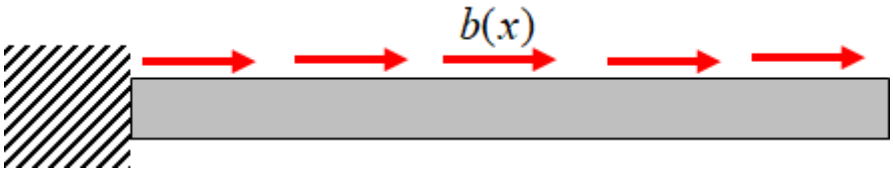

Figure 4. Rod subjected to fixed-free boundary condition and arbitrary distributed loading

The PD EoM and BCs for this case can be expressed as

$$\frac{2E}{\delta\varepsilon}\int_{-\varepsilon}^{\varepsilon}\frac{u(x+\xi)-u(x)}{|\xi|}d\xi+\frac{E}{\varepsilon^2}\left[\int_{-\delta}^{-\varepsilon}\left|\frac{\varepsilon^3}{\xi^3}\right|\frac{u(x+\xi)-u(x)}{|\xi|}d\xi+\int_{\varepsilon}^{\delta}\left|\frac{\varepsilon^3}{\xi^3}\right|\frac{u(x+\xi)-u(x)}{|\xi|}d\xi\right]+b(x)=0 \tag{40}$$

$$\begin{cases}u(-\xi)=-u(\xi)\\ u(L+\xi)=u(L-\xi)\end{cases}\quad 0\le\xi\le\delta \tag{41a, b}$$

Again, suppose the displacement function belongs to the vector space spanned by bases of trigonometric functions and hence can be expressed as

$$u(x)=\frac{a_0}{2}+\sum_{n=1}^{\infty}a_n\cos(s_nx)+b_n\sin(s_nx) \tag{42}$$

Using Eqs. (41a, b) one can obtain:

$$s_n=\frac{(2n-1)\pi}{2L} \tag{43}$$

and

$$u(x)=\sum_{n=1}^{\infty}b_n\sin\frac{(2n-1)\pi x}{2L} \tag{44}$$

Plugging Eq. (44) back into (40) and performing algebraic simplifications results in

$$\sum_{n=1}^{\infty}b_n\sin\frac{(2n-1)\pi x}{2L}\left\{\begin{array}{l}\dfrac{2E}{\delta\varepsilon}\displaystyle\int_{-\varepsilon}^{\varepsilon}\frac{1}{|\xi|}\left(\cos\frac{(2n-1)\pi\xi}{2L}-1\right)d\xi+\\ \dfrac{E}{\varepsilon^2}\left[\displaystyle\int_{-\delta}^{-\varepsilon}\left|\frac{\varepsilon^3}{\xi^4}\right|\left(\cos\frac{(2n-1)\pi\xi}{2L}-1\right)d\xi+\int_{\varepsilon}^{\delta}\left|\frac{\varepsilon^3}{\xi^4}\right|\left(\cos\frac{(2n-1)\pi\xi}{2L}-1\right)d\xi\right]\end{array}\right\}=-b(x) \tag{45}$$

where the coefficients can be determined as

$$b_n=-\frac{2}{L}\frac{\displaystyle\int_0^L b(x)\sin\frac{(2n-1)\pi x}{2L}dx}{\dfrac{2E}{\delta\varepsilon}\displaystyle\int_{-\varepsilon}^{\varepsilon}\frac{1}{|\xi|}\left(\cos\frac{(2n-1)\pi\xi}{2L}-1\right)d\xi+\frac{E}{\varepsilon^2}\left[\displaystyle\int_{-\delta}^{-\varepsilon}\left|\frac{\varepsilon^3}{\xi^4}\right|\left(\cos\frac{(2n-1)\pi\xi}{2L}-1\right)d\xi+\int_{\varepsilon}^{\delta}\left|\frac{\varepsilon^3}{\xi^4}\right|\left(\cos\frac{(2n-1)\pi\xi}{2L}-1\right)d\xi\right]} \tag{46}$$

Substituting Eq. (46) into (44) yields the PD analytical solution as

$$u(x)=-\sum_{n=1}^{\infty}\frac{2}{L}\frac{\displaystyle\int_0^L b(x)\sin\frac{(2n-1)\pi x}{2L}dx\sin\frac{(2n-1)\pi x}{2L}}{\dfrac{2E}{\delta\varepsilon}\displaystyle\int_{-\varepsilon}^{\varepsilon}\frac{1}{|\xi|}\left(\cos\frac{(2n-1)\pi\xi}{2L}-1\right)d\xi+\frac{E}{\varepsilon^2}\left[\displaystyle\int_{-\delta}^{-\varepsilon}+\int_{\varepsilon}^{\delta}\left|\frac{\varepsilon^3}{\xi^4}\right|\left(\cos\frac{(2n-1)\pi\xi}{2L}-1\right)d\xi\right]} \tag{47}$$

In particular when $\varepsilon=\delta$, Eq. (47) reduces to the analytical solution for traditional PD model as

$$u(x)=-\sum_{n=1}^{\infty}\frac{\delta^2}{LE}\frac{\displaystyle\int_0^L b(x)\sin\frac{(2n-1)\pi x}{2L}dx}{\displaystyle\int_{-\delta}^{\delta}\frac{1}{|\xi|}\left(\cos\frac{(2n-1)\pi\xi}{2L}-1\right)d\xi}\sin\frac{(2n-1)\pi x}{2L} \tag{48}$$

5. Analytical Solutions for Free Vibration Condition

5.1 Fixed-Fixed Rod

Let the PD EoM, BCs and ICs to be expressed for the fixed-fixed rod as:

$$\rho\frac{\partial^2u}{\partial t^2}(x,t)=\frac{2E}{\delta\varepsilon}\int_{-\varepsilon}^{\varepsilon}\frac{u(x+\xi)-u(x)}{|\xi|}d\xi+\frac{E}{\varepsilon^2}\left[\int_{-\delta}^{-\varepsilon}\left|\frac{\varepsilon^3}{\xi^3}\right|\frac{u(x+\xi)-u(x)}{|\xi|}d\xi+\int_{\varepsilon}^{\delta}\left|\frac{\varepsilon^3}{\xi^3}\right|\frac{u(x+\xi)-u(x)}{|\xi|}d\xi\right] \tag{49}$$

$$BCs:\begin{cases}u(-\xi,t)=-u(\xi,t)\\ u(L+\xi,t)=-u(L-\xi,t)\end{cases}\quad 0\le\xi\le\delta \tag{50a, b}$$

$$ICs:\begin{cases}u(x,0)=u_0(x)\\ \dfrac{\partial u}{\partial t}(x,0)=v_0(x)\end{cases} \tag{51a, b}$$

By using separation of variables approach, the displacement function can be decomposed as

$$u(x,t) = X(x)T(t) \tag{52}$$

Hence, Eq. (49) can be rewritten as

$$\rho X \frac{\partial^2 T}{\partial t^2} = T\left\{\frac{2E}{\delta\varepsilon}\int_{-\varepsilon}^{\varepsilon}\frac{X(x+\xi)-X(x)}{|\xi|}d\xi + \frac{E}{\varepsilon^2}\left[\int_{-\delta}^{-\varepsilon}\left|\frac{\varepsilon^3}{\xi^3}\right|\frac{X(x+\xi)-u(x)}{|\xi|}d\xi + \int_{\varepsilon}^{\delta}\left|\frac{\varepsilon^3}{\xi^3}\right|\frac{X(x+\xi)-u(x)}{|\xi|}d\xi\right]\right\} \tag{53}$$

Isolating variables yields:

$$\frac{\rho}{T}\frac{\partial^2 T}{\partial t^2} = \frac{1}{X}\left\{\frac{2E}{\delta\varepsilon}\int_{-\varepsilon}^{\varepsilon}\frac{X(x+\xi)-X(x)}{|\xi|}d\xi + \frac{E}{\varepsilon^2}\left[\int_{-\delta}^{-\varepsilon}\left|\frac{\varepsilon^3}{\xi^3}\right|\frac{X(x+\xi)-u(x)}{|\xi|}d\xi + \int_{\varepsilon}^{\delta}\left|\frac{\varepsilon^3}{\xi^3}\right|\frac{X(x+\xi)-u(x)}{|\xi|}d\xi\right]\right\} = -\lambda \tag{54}$$

which gives

$$\frac{2E}{\delta\varepsilon}\int_{-\varepsilon}^{\varepsilon}\frac{X(x+\xi)-X(x)}{|\xi|}d\xi + \frac{E}{\varepsilon^2}\left[\int_{-\delta}^{-\varepsilon}\left|\frac{\varepsilon^3}{\xi^3}\right|\frac{X(x+\xi)-u(x)}{|\xi|}d\xi + \int_{\varepsilon}^{\delta}\left|\frac{\varepsilon^3}{\xi^3}\right|\frac{X(x+\xi)-u(x)}{|\xi|}d\xi\right] = -\lambda X \tag{55a}$$

and

$$\rho\frac{\partial^2 T}{\partial t^2} + \lambda T = 0 \tag{55b}$$

By comparing Eq. (55a) with (25), we can consider $X(x)$ as an analogue to $u(x)$ and $\lambda X(x)$ to $b(x)$. Thus, associating with Eq. (33) and (36), one can obtain

$$X(x) = \sum_{n=1}^{\infty} b_n \sin\frac{n\pi x}{L} \tag{56}$$

and

$$\sum_{n=1}^{\infty} b_n \sin\left(\frac{n\pi x}{L}\right)\left\{\begin{array}{l}\dfrac{2E}{\delta\varepsilon}\displaystyle\int_{-\varepsilon}^{\varepsilon}\frac{1}{|\xi|}\left[\cos\left(\frac{n\pi\xi}{L}\right)-1\right]d\xi + \\ \dfrac{E}{\varepsilon^2}\left[\displaystyle\int_{-\delta}^{-\varepsilon}\left|\frac{\varepsilon^3}{\xi^4}\right|\left(\cos\frac{n\pi\xi}{L}-1\right)d\xi + \int_{\varepsilon}^{\delta}\left|\frac{\varepsilon^3}{\xi^4}\right|\left(\cos\frac{n\pi\xi}{L}-1\right)d\xi\right]\end{array}\right\} = -\sum_{n=1}^{\infty}\lambda_n b_n \sin\frac{n\pi x}{L} \tag{57}$$

which results in the PD ‘’eigenvalues’’ as

$$\lambda_n = \frac{2E}{\delta\varepsilon}\int_{-\varepsilon}^{\varepsilon}\frac{1}{|\xi|}\left[1-\cos\left(\frac{n\pi\xi}{L}\right)\right]d\xi + \frac{E}{\varepsilon^2}\left[\int_{-\delta}^{-\varepsilon}\left|\frac{\varepsilon^3}{\xi^4}\right|\left(1-\cos\frac{n\pi\xi}{L}\right)d\xi + \int_{\varepsilon}^{\delta}\left|\frac{\varepsilon^3}{\xi^4}\right|\left(1-\cos\frac{n\pi\xi}{L}\right)d\xi\right] \tag{58}$$

The general solution to Eq. (55b) can be expressed as

$$T_n(t) = A_n^* \cos\left(\sqrt{\frac{\lambda_n}{\rho}}t\right) + B_n^* \sin\left(\sqrt{\frac{\lambda_n}{\rho}}t\right) \tag{59}$$

Substituting Eq. (59) and (56) into (52) and rearranging the coefficient notations yields the general PD solution as

$$u(x,t)=\sum_{n=1}^{\infty}\left[A_n\cos\left(\sqrt{\frac{\lambda_n}{\rho}}t\right)+B_n\sin\left(\sqrt{\frac{\lambda_n}{\rho}}t\right)\right]\sin\frac{n\pi x}{L} \tag{60}$$

Differentiating Eq. (60) with respect to time yields:

$$\frac{\partial u}{\partial t}(x,t)=\sum_{n=1}^{\infty}\sqrt{\frac{\lambda_n}{\rho}}\left[-A_n\sin\left(\sqrt{\frac{\lambda_n}{\rho}}t\right)+B_n\cos\left(\sqrt{\frac{\lambda_n}{\rho}}t\right)\right]\sin\frac{n\pi x}{L} \tag{61}$$

Applying the ICs gives:

$$u(x,0)=u_0(x)\ \ \Rightarrow\ \ \sum_{n=1}^{\infty}A_n\sin\frac{n\pi x}{L}=u_0(x)\ \ \Rightarrow\ \ A_n=\frac{2}{L}\int_0^L u_0(x)\sin\frac{n\pi x}{L}dx \tag{62a}$$

$$\frac{\partial u}{\partial t}(x,0)=v_0(x)\ \ \Rightarrow\ \ \sum_{n=1}^{\infty}\sqrt{\frac{\lambda_n}{\rho}}B_n\sin\frac{n\pi x}{L}=v_0\ \ \Rightarrow\ \ B_n=\frac{2}{L}\sqrt{\frac{\rho}{\lambda_n}}\int_0^L v_0(x)\sin\frac{n\pi x}{L}dx \tag{62b}$$

As a summary, the PD analytical solution for free vibration of fixed-fixed rods can be summarized as

$$u(x,t)=\sum_{n=1}^{\infty}\left[A_n\cos\left(\sqrt{\frac{\lambda_n}{\rho}}t\right)+B_n\sin\left(\sqrt{\frac{\lambda_n}{\rho}}t\right)\right]\sin\frac{n\pi x}{L} \tag{63a}$$

$$\lambda_n=\frac{2E}{\delta\varepsilon}\int_{-\varepsilon}^{\varepsilon}\frac{1}{|\xi|}\left[1-\cos\left(\frac{n\pi\xi}{L}\right)\right]d\xi+\frac{E}{\varepsilon^2}\left[\int_{-\delta}^{-\varepsilon}\left|\frac{\varepsilon^3}{\xi^4}\right|\left(1-\cos\frac{n\pi\xi}{L}\right)d\xi+\int_{\varepsilon}^{\delta}\left|\frac{\varepsilon^3}{\xi^4}\right|\left(1-\cos\frac{n\pi\xi}{L}\right)d\xi\right] \tag{63b}$$

$$A_n=\frac{2}{L}\int_0^L u_0(x)\sin\frac{n\pi x}{L}dx \tag{63c}$$

$$B_n=\frac{2}{L}\sqrt{\frac{\rho}{\lambda_n}}\int_0^L v_0(x)\sin\frac{n\pi x}{L}dx \tag{63d}$$

In particular when $\varepsilon=\delta$, the PD ''eigenvalues'' reduce to

$$\lambda_n=\frac{2E}{\delta^2}\int_{-\delta}^{\delta}\frac{1}{|\xi|}\left[1-\cos\left(\frac{n\pi\xi}{L}\right)\right]d\xi \tag{63e}$$

which is valid for traditional PD model.

5.2 Fixed-Free Rod

Let the PD EoM, BCs and ICs for the fixed-free rod to be expressed as:

$$\rho\frac{\partial^2 u}{\partial t^2}(x,t)=\frac{2E}{\delta\varepsilon}\int_{-\varepsilon}^{\varepsilon}\frac{u(x+\xi)-u(x)}{|\xi|}d\xi+\frac{E}{\varepsilon^2}\left[\int_{-\delta}^{-\varepsilon}\left|\frac{\varepsilon^3}{\xi^3}\right|\frac{u(x+\xi)-u(x)}{|\xi|}d\xi+\int_{\varepsilon}^{\delta}\left|\frac{\varepsilon^3}{\xi^3}\right|\frac{u(x+\xi)-u(x)}{|\xi|}d\xi\right] \tag{64}$$

$$BCs:\begin{cases}u(-\xi,t)=-u(\xi,t)\\ u(L+\xi,t)=u(L-\xi,t)\end{cases}\quad 0\le\xi\le\delta \tag{65a, b}$$

$$ICs:\begin{cases} u(x,0)=u_0(x) \\ \dfrac{\partial u}{\partial t}(x,0)=v_0(x) \end{cases} \tag{66a, b}$$

By using separation of variables approach, i.e.,

$$u(x,t)=X(x)T(t) \tag{67}$$

two characteristic functions can be obtained by substituting Eq. (67) into (64) as

$$\frac{2E}{\delta\varepsilon}\int_{-\varepsilon}^{\varepsilon}\frac{X(x+\xi)-X(x)}{|\xi|}d\xi+\frac{E}{\varepsilon^2}\left[\int_{-\delta}^{-\varepsilon}\left|\frac{\varepsilon^3}{\xi^3}\right|\frac{X(x+\xi)-u(x)}{|\xi|}d\xi+\int_{\varepsilon}^{\delta}\left|\frac{\varepsilon^3}{\xi^3}\right|\frac{X(x+\xi)-u(x)}{|\xi|}d\xi\right]=-\lambda X \tag{68a}$$

and

$$\rho\frac{\partial^2 T}{\partial t^2}+\lambda T=0 \tag{68b}$$

By comparing Eq. (68a) with (40), we can consider $X(x)$ as an analogue to $u(x)$ and $\lambda X(x)$ to $b(x)$. Thus, associating with Eq. (44) and (45), one can obtain

$$X(x)=\sum_{n=1}^{\infty}b_n\sin\frac{(2n-1)\pi x}{2L} \tag{69a}$$

and

$$\sum_{n=1}^{\infty}b_n\sin\frac{(2n-1)\pi x}{2L}\left\{\begin{array}{l}\dfrac{2E}{\delta\varepsilon}\displaystyle\int_{-\varepsilon}^{\varepsilon}\frac{1}{|\xi|}\left[\cos\frac{(2n-1)\pi\xi}{2L}-1\right]d\xi+ \\ \dfrac{E}{\varepsilon^2}\left[\displaystyle\int_{-\delta}^{-\varepsilon}\left|\frac{\varepsilon^3}{\xi^4}\right|\left(\cos\frac{(2n-1)\pi\xi}{2L}-1\right)d\xi+\int_{\varepsilon}^{\delta}\left|\frac{\varepsilon^3}{\xi^4}\right|\left(\cos\frac{(2n-1)\pi\xi}{2L}-1\right)d\xi\right]\end{array}\right\}=-\sum_{n=1}^{\infty}\lambda_n b_n\sin\frac{(2n-1)\pi x}{2L} \tag{69b}$$

which results in the PD ‘’eigenvalues’’ as

$$\lambda_n=\frac{2E}{\delta\varepsilon}\int_{-\varepsilon}^{\varepsilon}\frac{1}{|\xi|}\left[1-\cos\frac{(2n-1)\pi\xi}{2L}\right]d\xi+\frac{E}{\varepsilon^2}\left[\int_{-\delta}^{-\varepsilon}\left|\frac{\varepsilon^3}{\xi^4}\right|\left(1-\cos\frac{(2n-1)\pi\xi}{2L}\right)d\xi+\int_{\varepsilon}^{\delta}\left|\frac{\varepsilon^3}{\xi^4}\right|\left(1-\cos\frac{(2n-1)\pi\xi}{L}\right)d\xi\right] \tag{70}$$

Similar to the derivations of the previous case, the refined PD analytical solution can be obtained as

$$u(x,t)=\sum_{n=1}^{\infty}\left[A_n\cos\left(\sqrt{\frac{\lambda_n}{\rho}}t\right)+B_n\sin\left(\sqrt{\frac{\lambda_n}{\rho}}t\right)\right]\sin\frac{(2n-1)\pi x}{2L} \tag{71a}$$

$$\lambda_n=\frac{2E}{\delta\varepsilon}\int_{-\varepsilon}^{\varepsilon}\frac{1}{|\xi|}\left[1-\cos\frac{(2n-1)\pi\xi}{2L}\right]d\xi+\frac{E}{\varepsilon^2}\left[\int_{-\delta}^{-\varepsilon}\left|\frac{\varepsilon^3}{\xi^4}\right|\left(1-\cos\frac{(2n-1)\pi\xi}{2L}\right)d\xi+\int_{\varepsilon}^{\delta}\left|\frac{\varepsilon^3}{\xi^4}\right|\left(1-\cos\frac{(2n-1)\pi\xi}{L}\right)d\xi\right] \tag{71b}$$

$$A_n=\frac{2}{L}\int_0^L u_0(x)\sin\frac{(2n-1)\pi x}{2L}dx \tag{71c}$$

$$B_n = \frac{2}{L}\sqrt{\frac{\rho}{\lambda_n}}\int_0^L v_0(x)\sin\frac{(2n-1)\pi x}{2L}dx \tag{71d}$$

In particular when $\varepsilon = \delta$, the PD ‘’eigenvalues’’ reduce to

$$\lambda_n = \frac{2E}{\delta^2}\int_{-\delta}^{\delta}\frac{1}{|\xi|}\left[1-\cos\frac{(2n-1)\pi\xi}{2L}\right]d\xi \tag{71e}$$

which is valid for the traditional PD model.

6. Numerical Results

6.1 Fixed-Fixed Rod Under Static Conditions

In the first case, a 1-Dimensional rod with a length of L = 1m is subjected to a body load of $b(x)$ =1000(1-x)^{10} N/m^3 under static conditions. Both edges of the rod are fixed (Fixed-Fixed). Elastic modulus of the rod is specified as E = 200 GPa.

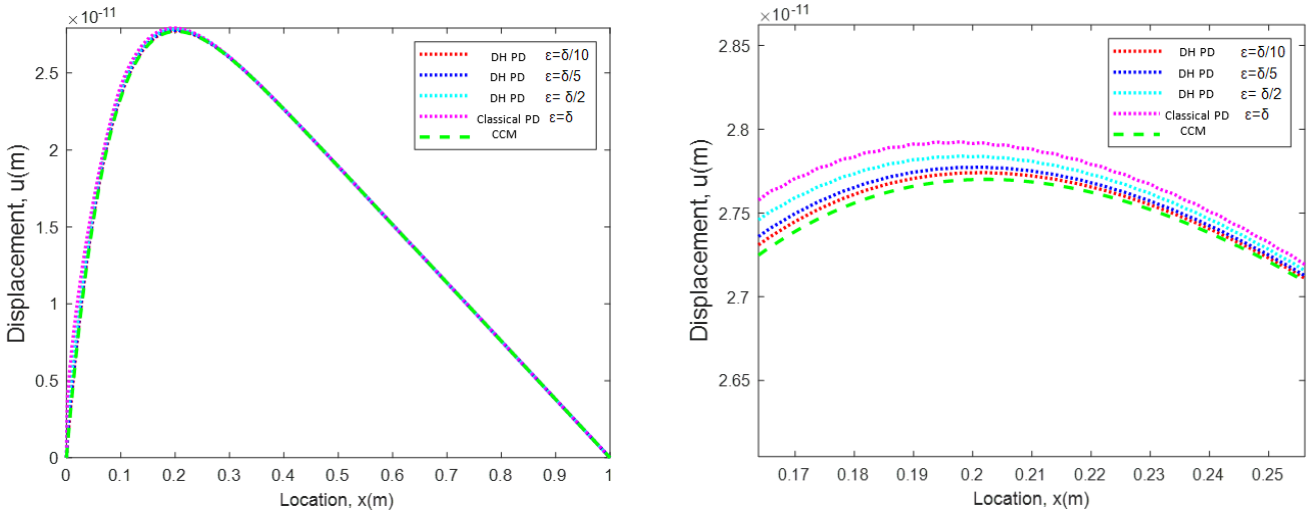

Figure 5. Variation of the displacement field along the rod by changing inner horizon size, ε, for a horizon value of δ = 0.1m.

Variation of the displacement field along the rod by changing inner horizon size, $\varepsilon = \delta, \delta/2, \delta/5, \delta/10$, for a horizon size value of δ = 0.1m are given in Fig. 5. As shown in this figure, as the size of the inner horizon decreases, double horizon peridynamic (DH PD) solution converges to the classical continuum mechanics solution.

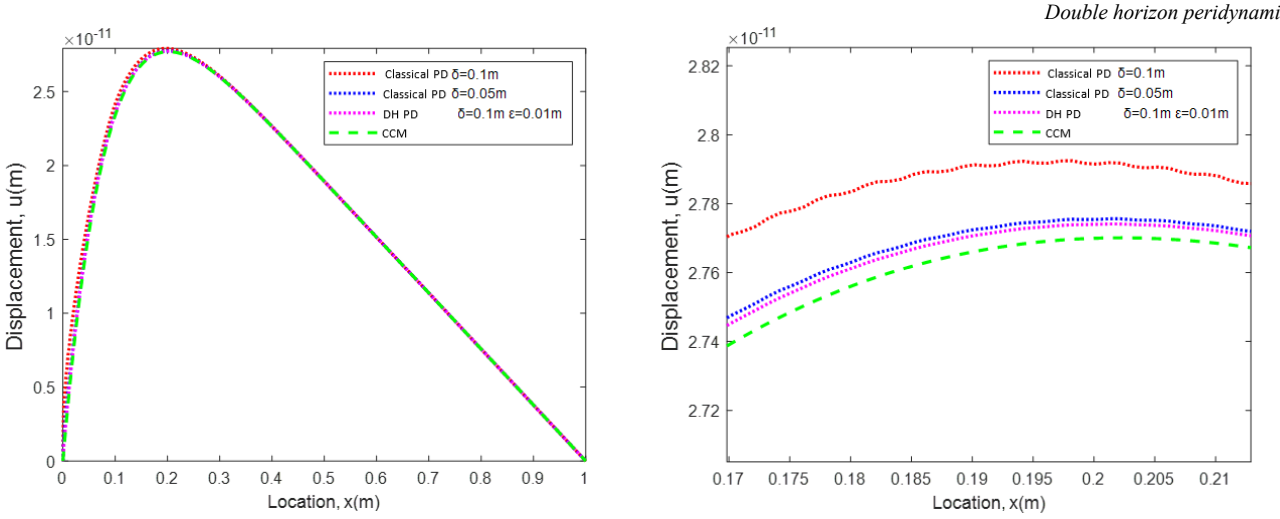

(a) **(b)**

Figure 6. Variation of the displacement field along the rod by changing the horizon size and using traditional or double horizon approach.

In Fig. 6, two different scenarios are compared. Firstly, as the horizon size decreases from $\delta = 0.1$ m to $\delta = 0.05$ m, peridynamic solution converges to the classical continuum mechanics solution as expected. On the other hand, even if a larger horizon size is used, i.e. $\delta = 0.1$ m, the new double horizon peridynamics (DH PD) approach provides closer results to CCM solution for an internal horizon size of, ε=0.01 m.

6.2 Fixed-Free Rod Under Static Conditions

In the second case, same properties are considered as in the first case except the right edge is left as free condition whereas the left edge is fixed under static conditions. First, the effect of the internal horizon size is investigated by changing the inner horizon size as, $\varepsilon = \delta, \delta/2, \delta/5, \delta/10$, for a horizon size value of $\delta = 0.1$m. As shown in Fig. 7, as the inner horizon size decreases, double horizon peridynamic (DH PD) results converge to the CCM solution based on the variation of displacements along the rod.

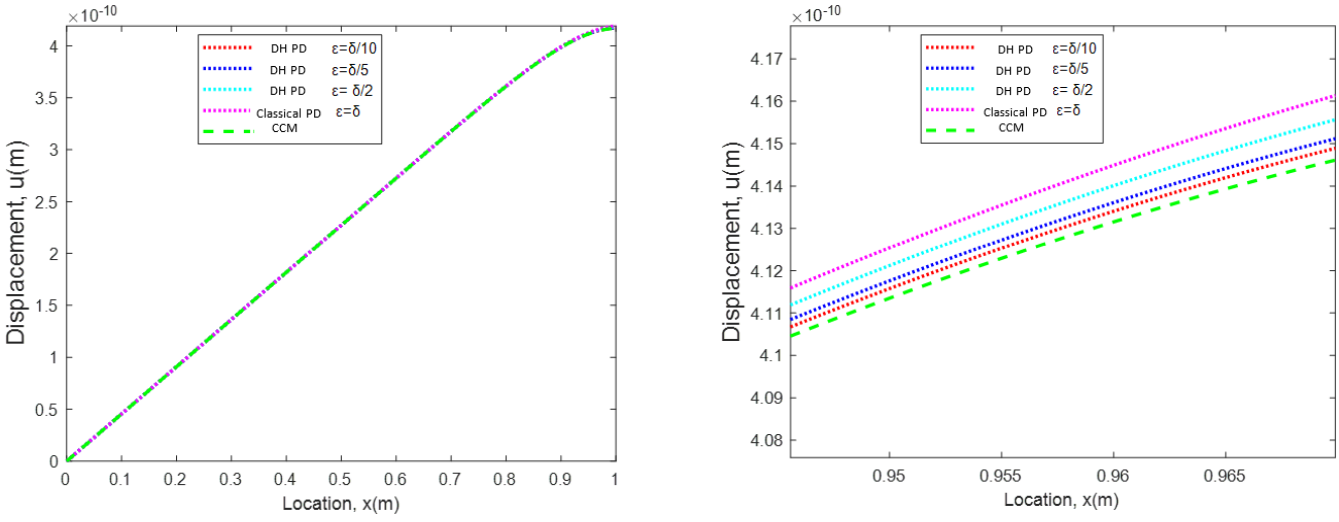

(a) **(b)**

Figure 7. Variation of the displacement field along the rod by changing inner horizon size, ε, for a horizon value of $\delta = 0.1$m.

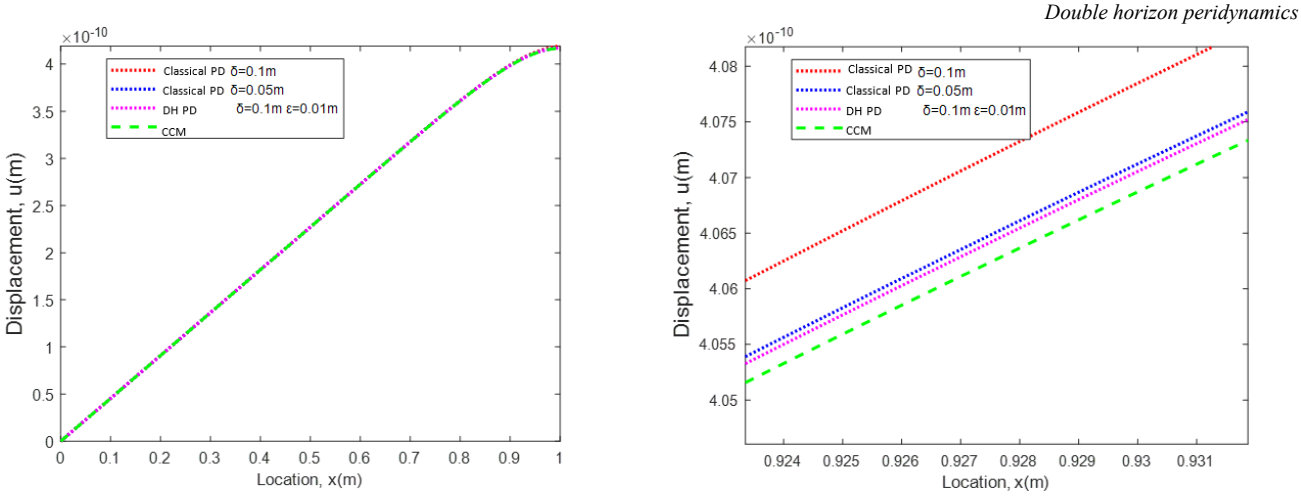

Figure 8. Variation of the displacement field along the rod by changing the horizon size and using traditional or double horizon approach.

Next, two different horizon size values are considered, $\delta = 0.1$ m, 0.05 m, by using traditional peridynamics and as expected, for the smaller horizon size value, peridynamic results are closer to CCM results (see Fig. 8). On the other hand, if double horizon peridynamic (DH PD) formulation is utilised, better agreement can be obtained even for a larger horizon size $\delta = 0.1$ m by considering the inner horizon size as $\varepsilon = 0.01$ m.

6.3 Fixed-Fixed Rod Under Free Vibration Conditions

In the third case, the capability of the double horizon peridynamic formulation under the dynamic free vibration conditions is investigated. The length of the rod is the same as the two previous cases. The horizon size is specified as $\delta = 0.1$m. Elastic modulus and density are given as $E = 200$ GPa and $\rho = 7850$ kg/m^3. Initial conditions are imposed as

$$u(x,0) = 0.01x^5(x-1)^5 \text{ m} \tag{72a}$$

$$\frac{\partial u}{\partial t}(x,0) = 10x^5(1-x)^5 \text{ m/s} \tag{72b}$$

As shown in Fig. 9, the variation of the displacement at the centre of the rod (x=0.5 m) as the time progresses is obtained by changing the internal horizon value as $\varepsilon = \delta, \delta/5, \delta/10, \delta/100$. Similar to the static cases, as the internal horizon size decreases, double horizon peridynamic (DH PD) results capture the CCM results very well for the same outer horizon size value which demonstrates the capability of the double horizon approach.

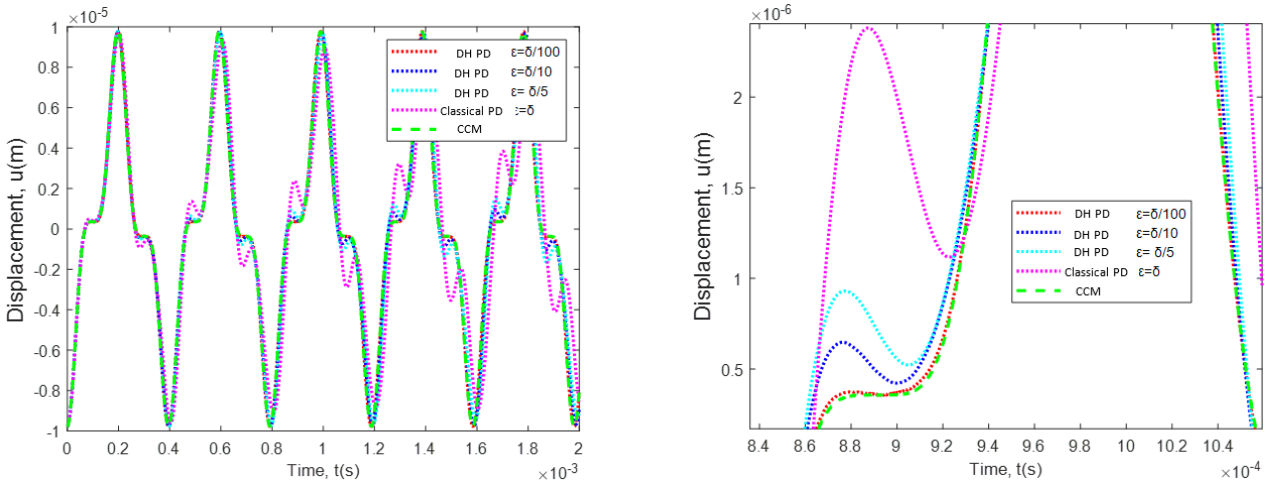

(a) **(b)**

Figure 9. Variation of the displacement field at the centre of the rod (x=0.5 m)by changing inner horizon size, ε, for a horizon value of δ = 0.1m.

6.4 Fixed-Free Rod Under Free Vibration Conditions

In the final numerical case, the same properties are considered as in the previous case except by assigning free condition for the right edge and fixed condition for the left edge under free vibration conditions and imposing the initial conditions as:

$$u(x,0) = 0.01x^5 \text{ m} \tag{73a}$$

$$\frac{\partial u}{\partial t}(x,0) = 0 \text{ m/s} \tag{73b}$$

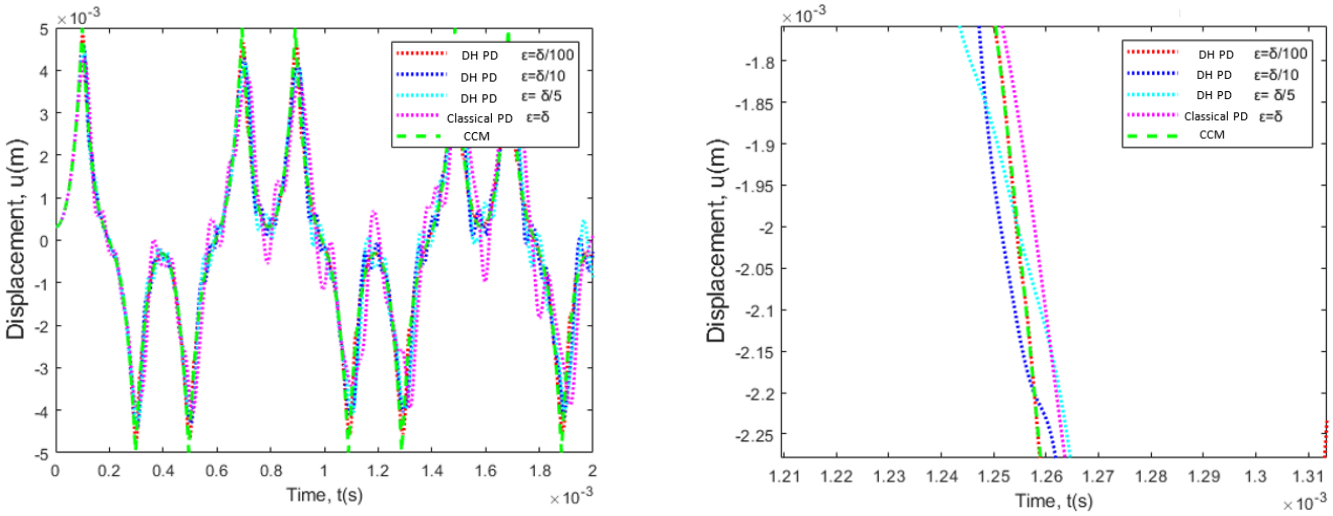

(a) **(b)**

Figure 10. Variation of the displacement field at the centre of the rod (x=0.5 m) by changing inner horizon size, ε, for a horizon value of δ = 0.1m.

As in the previous case, four different internal horizon values are considered as $\varepsilon = \delta$, $\delta/5$, $\delta/10$, $\delta/100$ and the variation of the displacement at the centre of the rod (x=0.5 m) is obtained as the time progresses as shown in Fig. 10. Similar to the previous case, double horizon peridynamic (DH PD) results match very well with the CCM results as the internal horizon size decreases.

7. Conclusions

In this study, a new double horizon peridynamics formulation was introduced by utilising two horizons instead of one as in traditional peridynamics. To demonstrate the capability of the current approach, four different numerical cases were examined by different boundary (fixed-fixed and fixed-free) and initial conditions under static and dynamic conditions for different outer and inner horizon size values. For both static and dynamic cases, it was observed that as the inner horizon decreases, peridynamic solutions converge to classical continuum mechanics solutions even by using a larger horizon size value. Therefore, the proposed approach can serve as an alternative approach to improve computational efficiency of peridynamic simulations by obtaining accurate results with larger horizon sizes. Potential future directions can be extending the current formulation to 2-Dimensional and 3-Dimensional models, and problems including fracture.

Acknowledgement

This material is based upon work supported by the Air Force Office of Scientific Research under award number FA9550-18-1-7004.

References

[1] Silling SA. Reformulation of elasticity theory for discontinuities and long-range forces. Journal of the Mechanics and Physics of Solids. 2000; 48(1):175-209.

[2] Madenci E, Oterkus E. *Peridynamic Theory and Its Applications*. New York: Springer, 2014.

[3] Oterkus E, Madenci E, Nemeth M. Stress analysis of composite cylindrical shells with an elliptical cutout. Journal of mechanics of materials and structures. 2007; 2(4): 695-727.

[4] Vazic B, Wang H, Diyaroglu C, Oterkus S, Oterkus E, 2017. Dynamic propagation of a macrocrack interacting with parallel small cracks. AIMS Materials Science. 2017; 4(1): 118-136.

[5] De Meo D, Russo L, Oterkus E. Modeling of the onset, propagation, and interaction of multiple cracks generated from corrosion pits by using peridynamics. Journal of Engineering Materials and Technology. 2017; 139(4): 041001.

[6] Imachi M, Tanaka S, Ozdemir M, Bui TQ, Oterkus S, Oterkus E. Dynamic crack arrest analysis by ordinary state-based peridynamics. International Journal of Fracture. 2020; 221(2): 155-169.

[7] Ozdemir M, Kefal A, Imachi M, Tanaka S, Oterkus E. Dynamic fracture analysis of functionally graded materials using ordinary state-based peridynamics. Composite Structures. 2020; 244: 112296.

[8] Liu X, He X, Wang J, Sun L, Oterkus E. An ordinary state-based peridynamic model for the fracture of zigzag graphene sheets. Proceedings of the Royal Society A: Mathematical, Physical and Engineering Sciences. 2018; 474(2217): 20180019.

[9] Huang Y, Oterkus S, Hou H, Oterkus E, Wei Z, Zhang S. Peridynamic model for visco-hyperelastic material deformation in different strain rates. Continuum Mechanics and Thermodynamics, 2022; 34(4): 977-1011.

[10] Diehl P, Prudhomme S, Lévesque M. A review of benchmark experiments for the validation of peridynamics models. Journal of Peridynamics and Nonlocal Modeling. 2019; 1(1): 14-35.

[11] Zhou XP, Yao WW. Smoothed bond-based peridynamics. Journal of Peridynamics and Nonlocal Modeling, 2021; 1-23.

[12] Prakash N, Stewart RJ. A multi-threaded method to assemble a sparse stiffness matrix for quasi-static solutions of linearized bond-based peridynamics. Journal of Peridynamics and Nonlocal Modeling. 2021; 3(2): 113-147.

[13] Naumenko K, Pander M, Würkner M. Damage patterns in float glass plates: Experiments and peridynamics analysis. Theoretical and Applied Fracture Mechanics. 2022; 118: 103264.

[14] Yan H, Jivkov AP, Sedighi M. Modelling soil desiccation cracking by peridynamics. Géotechnique. 2022; 1-13.

[15] Hidayat MIP, Lemma TA and Machmudah A. A review on connection between meshfree peridynamics and meshfree methods. In AIP Conference Proceedings. 2021; 2384(1): 030006.

[16] Guski V, Verestek W, Rapp D, Schmauder S. Microstructural investigation of plasma sprayed ceramic coatings focusing on the effect of the splat boundary for SOFC sealing applications using peridynamics. Theoretical and Applied Fracture Mechanics. 2021; 112: 102926.

[17] Kefal A, Sohouli A, Oterkus E, Yildiz M, Suleman A. Topology optimization of cracked structures using peridynamics. Continuum Mechanics and Thermodynamics. 2019; 31(6): 1645-1672.

[18] Yang Z, Vazic B, Diyaroglu C, Oterkus E, Oterkus S. A Kirchhoff plate formulation in a state-based peridynamic framework. Mathematics and Mechanics of Solids. 2020; 25(3): 727-738.

[19] Yang, Z, Oterkus E, Oterkus S. Peridynamic higher-order beam formulation. Journal of Peridynamics and Nonlocal Modeling. 2021; 3(1): 67-83.

[20] Yang Z, Oterkus E, Oterkus S. Peridynamic formulation for higher-order plate theory. Journal of Peridynamics and Nonlocal Modeling. 2021; 3(3): 185-210.

[21] Yang Z, Oterkus S, Oterkus E. Peridynamic formulation for Timoshenko beam. Procedia Structural Integrity. 2020; 28: 464-471.

[22] Yang Z, Oterkus E, Oterkus S. A novel peridynamic mindlin plate formulation without limitation on material constants. Journal of Peridynamics and Nonlocal Modeling. 2021; 3(3): 287-306.

[23] Yang Z, Oterkus E, Oterkus S. A state-based peridynamic formulation for functionally graded Euler-Bernoulli beams. CMES-Computer Modeling in Engineering and Sciences. 2020; 124(2): 527-544.

[24] Yang Z, Oterkus E and Oterkus S. Analysis of functionally graded Timoshenko beams by using peridynamics. Journal of Peridynamics and Nonlocal Modeling. 2021; 3(2): 148-166.

[25] Yang Z, Oterkus E, Oterkus S. Peridynamic modelling of higher order functionally graded plates. Mathematics and Mechanics of Solids. 2021; 26(12): 1737-1759.

[26] Yang Z, Oterkus E, Oterkus S. A state-based peridynamic formulation for functionally graded Kirchhoff plates. Mathematics and Mechanics of Solids. 2021; 26(4): 530-551.

[27] Yang Z, Oterkus E, Oterkus S. Peridynamic formulation for higher order functionally graded beams. Thin-Walled Structures. 2021; 160: 107343.

[28] Dorduncu M, Olmus I, Rabczuk T. A peridynamic approach for modeling of two dimensional functionally graded plates. Composite Structures. 2022; 279: 114743.

[29] Dorduncu M. Peridynamic modeling of delaminations in laminated composite beams using refined zigzag theory. Theoretical and Applied Fracture Mechanics. 2021; 112: 102832.

[30] Kutlu A, Dorduncu M and Rabczuk T. A novel mixed finite element formulation based on the refined zigzag theory for the stress analysis of laminated composite plates. Composite Structures. 2021; 267: 113886.

[31] Mikata Y. Peridynamics for fluid mechanics and acoustics. Acta Mechanica. 2021; 232(8): 3011-3032.

[32] Diyaroglu C, Oterkus S, Oterkus E, Madenci E, Han S and Hwang Y. Peridynamic wetness approach for moisture concentration analysis in electronic packages. Microelectronics Reliability. 2017; 70: 103-111.

[33] Martowicz A, Kantor S, Pieczonka Ł, Bryła J and Roemer J. Phase transformation in shape memory alloys: a numerical approach for thermomechanical modeling via peridynamics. Meccanica. 2021; 56(4): 841-854.

[34] Dorduncu M and Madenci E. Finite element implementation of ordinary state-based peridynamics with variable horizon. Engineering with Computers. 2022; 1-14.

[35] Madenci E, Dorduncu M, Phan N and Gu, X. Weak form of bond-associated non-ordinary state-based peridynamics free of zero energy modes with uniform or non-uniform discretization. Engineering Fracture Mechanics. 2019; 218: 106613.

[36] Bobaru F and Hu W. The meaning, selection, and use of the peridynamic horizon and its relation to crack branching in brittle materials. International Journal of Fracture. 2012; 176: 215-222.

[37] Wang B, Oterkus S and Oterkus E. Determination of horizon size in state-based peridynamics. Continuum Mechanics and Thermodynamics. 2020; 1-24.

[38] Ren H, Zhuang X and Rabczuk T. Dual-horizon peridynamics: A stable solution to varying horizons. Computer Methods in Applied Mechanics and Engineering. 2017; 318: 762-782.

[39] Ren H, Zhuang X, Cai Y and Rabczuk T. Dual-horizon peridynamics. International Journal for Numerical Methods in Engineering. 2016; 108(12): 1451-1476.

[40] Wang B, Oterkus S and Oterkus E. Derivation of dual-horizon state-based peridynamics formulation based on Euler–Lagrange equation. Continuum Mechanics and Thermodynamics. 2020; 1-21.

[41] Wang B, Oterkus S and Oterkus E. Thermal diffusion analysis by using dual horizon peridynamics. Journal of Thermal Stresses. 2020; 44(1): 51-74.